Surface Science 656 (2017) 24–32

Contents lists available at ScienceDirect

Surface Science

journal homepage: www.elsevier.com/locate/susc

Adsorption and dissociation of molecular hydrogen on orthorhombic β-Mo_2C and cubic δ-MoC (001) surfaces

Sergio Posada-Pérez[a], Francesc Viñes[a,*], Rosendo Valero[a], José A. Rodriguez[b], Francesc Illas[a]

[a] Departament de Ciència de Materials i Química Física & Institut de Química Teòrica i Computacional (IQTCUB), Universitat de Barcelona, c/ Martí i Franquès 1, 08028 Barcelona, Spain

[b] Chemistry Department, Brookhaven National Laboratory, Upton, NY 11973, USA

ARTICLE INFO

Keywords:
Density functional calculations
Molybdenum carbides
H_2 dissociation
Ab initio thermodynamics
IR spectroscopy
Core level shifts

ABSTRACT

Molybdenum carbides are increasingly used in heterogeneously catalyzed hydrogenation reactions, which imply the adsorption and dissociation of molecular hydrogen. Here a systematic density functional theory based study, including or excluding dispersion terms, concerning the interaction and stability of H_2 with cubic δ-MoC(001) and orthorhombic β-Mo_2C(001) surfaces, is presented. In the latter case the two possible C or Mo terminations are considered. In addition, different situations for the H covered surfaces are examined. Computational results including dispersive forces predict an essentially spontaneous dissociation of H_2 on β-Mo_2C(001) independently of the surface termination, whereas on δ-MoC(001) molecular hydrogen dissociation implies a small but noticeable energy barrier. Furthermore, the *ab initio* thermodynamics formalism has been used to compare the stability of different H coverages. Finally, core level binding energies and vibrational frequencies are presented with the aim to assist the interpretation of yet unavailable data from X-ray photoelectron and infrared spectroscopies.

1. Introduction

The pioneering work of Levy and Boudart [1] showing that, for a variety of reactions, the catalytic activity of WC is similar or even better than that of platinum, triggered a number of studies dealing with reactions catalyzed by early transition metal carbides (TMCs) [2–5]. The interest on the catalytic properties of TMCs surfaces has been accompanied by a significant number of surface science studies [3,6,7]. Nevertheless, one must realize that, in some cases, preparing well-defined single crystal surfaces can be extremely difficult. This is for instance the case of δ-MoC, which, due to the complex phase diagram of MoC [7], is usually found in the form of polycrystalline samples. It is important to point out that, in addition to their remarkable catalytic [8] and electrocatalytic [9] activities, TMCs are widely used in different applications due to their appealing chemical properties such as extreme hardness [10], excellent electric and thermal conductivities [2], and high melting points [11].

In the past ten years the catalytic activity of the different available TMCs has been investigated for several reactions, either as the active phase or as support [12–14]. Owing to their activity and the fact that they do not require special conditions for their synthesis [15], Mo carbides have stood out among other TMCs. Very recently it has been shown that the interaction of ethylene with δ-MoC(001) and Pt(111) exhibits a similar adsorption energy [16], further reinforcing the idea that early TMCs exhibit chemical features of late transition metals. On the other hand, Mo_2C phases have been proposed as alternative to commercial catalyst for water gas shift reaction (WGS) [17] and Pt/Mo_2C based catalyst also display very high rates for WGS [18]. Mo_2C is also active for the hydrogenation of dimethyl oxalate towards ethanol [19], the hydrodeoxygenation of butiric acid [20], the formic acid decomposition to CO and H_2 [21], CO_2 reduction [4,22], and its conversion to CO, CH_4, methanol, or ethanol [23–25], although a very recent study showed that MoC, Cu/MoC, and Au/MoC are more selective and stable catalysts than Mo_2C, Cu/Mo_2C, and Au/Mo_2C for CO_2 conversion [26]. Furthermore, steam reforming catalysis has been recently theoretically tackled using δ-MoC and β-Mo_2C [27].

Many of these chemical reactions involve hydrogenation and/or dehydrogenation steps. Hence, the relative stability of the different phases of the Mo carbides in absence/presence of H_2 is also an important issue to evaluate their possible use in hydrogenation reactions. Likewise, the study of the H_2 adsorption/desorption and H_2 dissociation/formation elementary steps is important since these are common and determinant ones and, therefore, understanding the molecular mechanisms involved in these pathways is essential to reach

* Corresponding author.
E-mail address: francesc.vines@ub.edu (F. Viñes).

http://dx.doi.org/10.1016/j.susc.2016.10.001
Received 18 August 2016; Received in revised form 27 September 2016; Accepted 2 October 2016
Available online 03 October 2016

a complete picture of the underlying chemistry. The objective of the present study is precisely to carry out a systematic theoretical work about the interaction of H_2 with (001) surfaces of orthorhombic Mo_2C and cubic MoC carbides. This work also aims to complement a recent study published by Wang and coworkers [28] where the stability of different terminations of orthorhombic Mo_2C at different H coverages is exhaustively studied within the framework of *ab initio* thermodynamics [29,30]. We report these results also including the stability of δ-MoC and, in addition, analyzing H_2 adsorption and its dissociation/formation providing as well estimates of C 1*s* core level binding energy shifts and vibrational fingerprints to assist the interpretation of forthcoming data from X-ray photoelectron (XPS) and infrared spectroscopies (IR).

2. Computational details

First of all, and in order to avoid any possible misunderstanding arising from the different notations used in the literature for molybdenum carbides, it is necessary to highlight that here we follow the notation convention defined by the joint committee on power diffraction standards (JCPDS) data files [31]. This notation is the same used in our previous work [32] and also by others [33]. So, hexagonal and orthorhombic Mo_2C crystal structures are denoted as α-Mo_2C and β-Mo_2C, respectively. Note, however, that some authors in the literature refer to orthorhombic Mo_2C as α-Mo_2C [34–36], following an early definition by Christensen [37]. In the case of MoC, the cubic phase is always referred to as δ-MoC. The space group for β-Mo_2C is *Pbcn* [38] and for cubic δ-MoC is $Fm\bar{3}m$. In all cases, the (001) surface is considered and represented by suitable slab models. These contain four atomic layers and involve a (2×2) supercell. In the case of β-Mo_2C, two possible terminations are possible for the (001) surface exposing either C or Mo atoms to the vacuum. Hereafter these surfaces are referred to as β-C and β-Mo, respectively.

The periodic density functional calculations (DFT) were performed using the Perdew-Burke-Ernzerhof (PBE) exchange-correlation functional [39], neglecting or including van der Waals interactions. In the latter case, the method proposed by Grimme (D2) [40] has been chosen. The electronic density of the valence electrons is expanded in a plane-wave basis set and the effect caused by the core electrons on those in the valence region is described by the projected augmented wave (PAW) method of Blöch [41] as implemented by Kresse and Joubert [42]. Numerical integration in the reciprocal space was carried out using 3×3×1 and 5×5×1 Monkhorst-Pack **k**-points grids [43] for δ-MoC and β-Mo_2C slabs, respectively. These settings are as in our previous work, where the stability of different surfaces of these carbides has been studied in detail, finding them suited to provide highly-accurate results [32]. An electronic relaxation criterion of 10^{-5} eV was used, and the atomic positions were allowed to relax until forces acting on atoms were always smaller than 0.01 eV $Å^{-1}$. Transition state structures have been located using the Dimer method [44] and characterized *via* frequency analysis of the modes related to the adsorbate expand the description presented in previous works [45]. In all cases calculations have been carried out by fully relaxing the two outermost atomic layers whereas the two bottommost were fixed as in the bulk to provide an adequate environment to the atoms in the surface region. The energies have been corrected using zero point energy (ZPE) taking into account the vibrations of the gas phase and the adsorbates. All DFT calculations were carried out using the VASP code [46]. The adsorption site nomenclature is detailed in Refs. [23,47].

Furthermore, we used the *ab initio* thermodynamics formalism proposed by Reuter and Scheffler [29,30] to estimate the surface free energy after H adsorption (γ^{cover})—Gibbs adsorption energy per surface area—at different hydrogen coverages (*N*) and as a function of pressure (*p*) and temperature (*T*). The γ^{cover} can be calculated as the sum of the surface free energy of the clean surface (γ^{clean}) plus the Gibbs free energy related with the adsorption of H atoms (γ^{ads}), both of them normalized per surface area, following Eq. (1).

$$\gamma^{cover}(T, p, N)=\gamma^{clean}(T, p)+\gamma^{ads}(T, p, N) \quad (1)$$

Following Reuter and Scheffler [29,30], the surface free energy of a clean surface as function of *p* and *T* can be obtained using Eq. (2):

$$\gamma^{clean}(T, p)=\frac{1}{A}\left[G^{clean}(T, p)-\sum_i N_i\mu_i(T, p)\right] \quad (2)$$

where G^{clean} is the Gibbs free energy of the surface, $\mu_i(T, p)$ is the chemical potential of the *i* species which form the solid surface, $N_i$is the number of atoms of element *i*, and *A* is the total surface area. For Mo_xC carbides surfaces, one can adapt Eq. (2) as shown on Eq. (3).

$$\gamma^{clean}(T, p)=\frac{1}{A}[G^{slab}_{Mo_xC}-N_C\mu_C(T, p)-N_{Mo}\mu_{Mo}(T, p)] \quad (3)$$

where $G^{slab}_{Mo_xC}$ is the Gibbs free energy of δ-MoC or β-Mo_2C surfaces and μ_C and μ_{Mo} are the chemical potentials of C and Mo atoms, normally obtained using graphite and Mo bulk references, respectively [28,48]. The N_C and N_{Mo} terms are the number of C and Mo atoms on the surfaces. Here, one has to point out that the slab models used in the present work contain four layers, two of them fixed and the other two relaxed. This fact leads to different energy values depending on the surface termination or require using a different model to estimate the γ^{clean} term. For this reason, we approximate γ^{clean} as the surface energy predicted in previous works [32]. In the case of Mo- and C-terminated β-Mo_2C surfaces we used instead the cleavage energies computed as proposed by Moreira and coworkers [49]. This is because estimating the surface energy of slabs with two differently terminated surfaces is cumbersome [50]. Note that by using these surface energy values, the chemical potential of C and Mo atoms does not need to be taken into account. Instead, the calculated values are referred to MoC and Mo_2C bulk materials.

Aside, the adsorption Gibbs free energy [$\gamma^{ads}(T, p, N)$] can be estimated as in Eq. (4).

$$\gamma^{ads}(T, p, N_H)=\frac{1}{A}[G^{cover}(T, p, N_H)-G^{slab}_{Mo_xC}(T, p)-G^{H_2}(T, p)] \quad (4)$$

where $G^{cover}(T, p, N_H)$ is the Gibbs energy of the H covered surface at *T*, *p*, and containing N_H hydrogen atoms, and $G^{H_2}(T, p)$ the Gibbs energy of the H_2 molecule also at *T* and *p*. In addition, the $G^{cover}(T, p, N_H)$ and $G^{slab}_{Mo_xC}(T, p)$ terms can be obtained from the DFT energy of the covered and clean slabs since

$$G^{cover}(T, p, N_H)=(E^{cover}-TS^{cover}+pV) \quad (5)$$

$$G^{slab}_{Mo_xC}(T, p)=(E^{slab}_{Mo_xC}-TS^{slab}_{Mo_xC}+pV) \quad (6)$$

where E^{cover} and $E^{slab}_{Mo_xC}$are the total energy of the systems (covered and clean) obtained from the corresponding DFT based calculations (E^{total}) plus the zero point vibrational energy (E^{O}), S^{cover} and $S^{slab}_{Mo_xC}$ are the corresponding entropy values, and *pV* is the pressure-volume term. Both entropy and *pV* terms are usually neglected. Note, in fact, that for a cell dimension of 10×10×10 Å and an external pressure of 10^5 Pa, the contribution of *pV* term is 1 meV, and a similar argument applies to the entropy term [29,30]. Therefore, Gibbs free energy of clean and H covered surfaces are represented by the total energy of clean (E^{clean}) and covered (E^{cover}) surfaces obtained by DFT calculations, whereas the Gibbs energy for the gas takes into account all thermodynamic contributions. With these approximations one can estimate the adsorption surface free energy (γ^{ads}) as in Eq. (7).

$$\gamma^{ads}(p, T, N_H)\frac{1}{A}\left[E^{cover}-E^{slab}_{Mo_xC}-N_H\left(\frac{E_{H_2}}{2}+\frac{E^{ZPE}_{H_2}}{2}+\Delta\mu_{0_{H_2}}+k_BT\ln\frac{p}{P_0}\right)\right] \quad (7)$$

where E_{H_2} is the DFT total energy of H_2 molecule in vacuum, $E^{ZPE}_{H_2}$ is its

zero point energy correction, k_B is the Boltzmann constant, p is the working pressure and $\Delta\mu_{0_{H_2}}$ is the chemical potential of H_2 calculated as in Eq. (8).

$$\Delta\mu_{0_{H_2}} = -\frac{1}{2}k_b T \ln Q_{Total} \quad (8)$$

where Q_{Total} is the sum of the electronic, rotational, translational, and vibrational partition functions of the gas phase H_2 molecule. Note that the definition in Eq. (8) implicitly contains a dependence on p and T.

Regarding to the predictions concerning core level binding energy shifts (ΔCLBE), two different approximations are often used in theoretical calculations using either Hartree-Fock (HF) [51–53] or DFT based approaches [54–56]. On one hand, one has the initial state approximation, which computes CLBEs without taking into account the electron density relaxation effect upon one core electron ionization. Here, a ground state calculation is necessary without considering the core hole effect. The CLBE in the initial state approach requires computing the energy of the core hole ionized system using the density of the neutral molecule. It has been also claimed that initial state values for CLBEs can be derived from the Kohn-Sham eigenvalues. This has, however, proven to be incorrect although Kohn-Sham eigenvalues nicely follow the trends of ΔCLBEs with respect to a given reference [56]. Here, ΔCLBEs for the C 1*s* of the MoC and Mo_2C surfaces at different hydrogen coverage have been computed relying on the PAW eigenvalues energy (E_C) computed with respect to the Fermi level (E_F), as in Eq. (9).

$$BE = E_F - E_C \quad (9)$$

On the other hand, a more accurate estimate of CLBEs or ΔCLBEs requires taking into account the relaxation of the core and valence electron density in response to the creation of the core hole; this is usually referred to as final state contribution and CLBEs including the final state contribution are broadly described final state approaches. Strictly speaking, to obtain the final state contribution it is necessary to carry out variational calculations for the system in the ground state and for the system with a core hole. The procedure is usually referred to as ΔSCF no matter whether the SCF calculation is of HF or DFT type [56]. For periodic systems, where the core electrons are often described with a pseudopotential, ΔSCF calculations are far from being straightforward and further simplifications are usually made.

One way is to mimic a core hole ionization by a corresponding core excited pseudopotential generated on-the-fly and the missing electron added to the valence band to keep the system neutrality. These approximations may cause errors in absolute values of the calculated CLBEs and thus only ΔCLBE relative shifts are meaningful as in the case of initial state approximation [56]. Kölher and Kresse argued that, in this approximation, the shifts between the bulk and surface are expected to agree with the experiments because, in metallic systems, the valence electrons rapidly screen the core hole [57]. Therefore, to avoid the above described problem related to the use of ΔSCF calculations in periodic systems, we rely on initial state values only and obtain ΔCLBEs relative to the bulk C(1*s*) CLBE of δ-MoC and of β-Mo_2C. Therefore, ΔCLBE values have been computed as in Eq. (10),

$$\Delta\text{CLBE} = (E_F - E_C) - (E_{F-Bulk} - E_{C-Bulk}) \quad (10)$$

where E_{F-Bulk} is the Fermi level of the bulk carbide and E_{C-Bulk} stands for the Kohn-Sham eigenvalue of the core state. The bulk systems have been calculated using the same criteria as surfaces optimizations, except for the 5×5×5 **k**-points grid as is in a previous work [32].

Vibrational frequencies related to adsorbed H atoms have been obtained within the harmonic approximation by explicit diagonalization of the Hessian block matrix involving only adsorbate coordinates. The corresponding matrix elements of the Hessian matrix are obtained as finite differences of 0.03 Å. The intensity of each normal mode has been obtained from the vibration corresponding dipole moment change normal to surface.

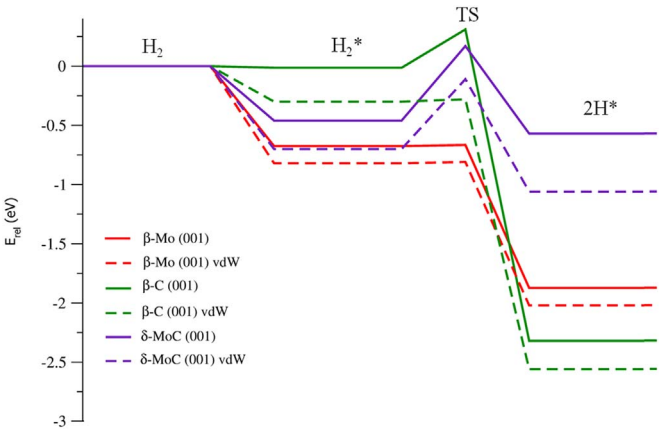

Fig. 1. Energy profile of H_2 adsorption and dissociation including ZPE correction on β-Mo, β-C, and δ-MoC (001) surfaces including vdW terms (dashed lines) or not (solid lines).

3. Results and discussion

In this section we describe the results for the systems of interest. To ease the discussion and better focus on the different calculated and predicted values, separate subsection are used.

3.1. Hydrogen adsorption and dissociation

Fig. 1 displays the ZPE energy profile for H_2 dissociation on the different Mo_nC (001) studied surfaces including or not the vdW correction. Furthermore, Table 1 summarizes the reaction energy values (ΔE), and the H_2 dissociation (E_b) and formation (E_{br}) energy barriers. On Fig. 2, the sketches of H_2 and 2H* adsorptions, as well as of H_2 dissociation transition states (TS), are shown for calculations including vdW dispersion; the frequency analysis is shown on Table S1 of the Supplementary material. It is worth mentioning that, except in the case of the β-Mo surface, and due to cancelling effects, results including vdW interactions are markedly different from those neglecting them. Therefore, to describe H_2 adsorption and dissociation on these surfaces, dispersion terms should be taken into account. The adsorption data of H_2 molecule and 1H isolated atom are displayed on Table S2 and S3, respectively.

In the case of the β-Mo surface, both approaches describe the H_2 dissociation as an essentially spontaneous process. The H_2 adsorption energy presents a difference of 0.15 eV between calculations with or without vdW dispersion, and the same difference is found for the two adsorbed hydrogen atoms. Thus, the calculated energy barrier for the H_2 formation including or not dispersion is the same (1.20 eV). Therefore, these results indicate that vdW dispersion does not play particularly a crucial role on the H_2 energy profile on β-Mo, probably owing to the fact that the electronic interaction between β-Mo and H_2 molecule is already strong (−0.67 eV), and vdW dispersion is usually used for describing very weak interactions.

Regarding β-C surface, the calculations without vdW dispersion show a very weak interaction between H_2 and β-C surface (−0.02 eV)

Table 1
H_2 adsorption energy (E_{ads}), dissociation energy (ΔE), dissociation energy barrier (E_b), and H_2 formation energy barrier (E_{rb}), including vdW dispersion or not, on β-Mo, β-C, and δ-MoC (001) surfaces. All energies are given in eV.

	non-vdW				vdW			
	E_{ads}	ΔE	E_b	E_{rb}	E_{ads}	ΔE	E_b	E_{rb}
β-Mo	−0.67	−1.20	~0	1.20	−0.82	−1.20	~0	1.20
β-C	−0.02	−2.31	0.32	2.63	−0.30	−2.26	~0	2.27
δ-MoC	−0.46	−0.11	0.64	0.75	−0.70	−0.35	0.60	0.96

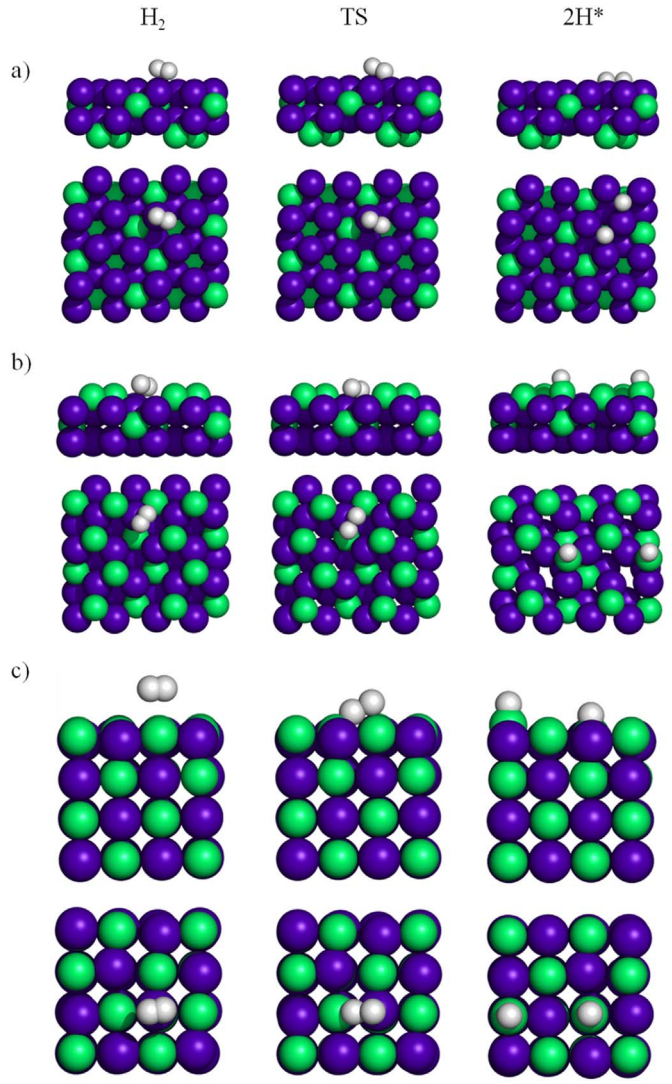

Fig. 2. Sketches on side view (top) and top view (bottom) of H_2 adsorption (left), TS (middle), and 2H* adsorption (right) on β-Mo (a), β-C (b), and δ-MoC (c) (001) surfaces. Pictures correspond to calculations including vdW dispersion. Violet, green, and white balls represents Mo, C, and H atoms, respectively. (For interpretation of the references to color in this figure legend, the reader is referred to the web version of this article.)

and an energy barrier of 0.33 eV for the H–H bond cleavage. Therefore, H_2 desorption is favored with respect to dissociation, and, consequently, these results would seem to indicate that the H_2 dissociation — a necessary step for many hydrogenation processes— would only occur on the β-Mo termination. However, calculations explicitly including the vdW terms predict a physisorption state with an adsorption energy of −0.30 eV with an essentially zero barrier for dissociation, as in the case of the β-Mo surface. This computational result would then suggest that H_2 dissociation is likely to occur on both surface terminations. Since in the case of the β-C surface the interaction with H_2 is very weak, the inclusion of vdW terms becomes unavoidable. Similar conclusions were obtained for methane adsorption on the same surfaces [47]. Not unexpectedly, the adsorbate molecular geometry remains unchanged [16,47].

Another remarkable fact is the high exothermicity of H_2 dissociation on β-C, where calculations including or not dispersion predict the formation of strong C–H bonds (1.10 Å). Furthermore, the low coverage H adsorption on β-C surface also implies surface reconstruction, due to the displacement of the CH moieties from the initial position to the vicinal Hollow Mo^2 sites. This C redistribution, which is observed in previous works with CO_2 as an adsorbate [23], stabilizes the surface energy increasing the exothermicity of the H adsorption process. The energy difference between reconstructed and non-reconstructed surface after the H adsorption is around 0.8 eV. In the recent work of Wang et al. [28] this surface reconstruction was not reported, and for this reason the adsorption energy of 2H* atoms on β-Mo was found to be favorable with respect the adsorption on β-C, opposite to present results.

Notice that the reverse process (H_2 formation) would imply an energy barrier of 2.27 eV, due to the high stability of the formed C–H bonds. This fact also suggests that, in spite of the low energy barrier for H_2 dissociation, the hydrogenation catalytic activity would be smaller since H adatoms are strongly bound to the surface. In comparison to H_2 adsorption on hexagonal α-Mo_2C phase [58], the H_2 dissociation was also to be very exothermic and involved very low energy barriers (0.34 eV at worst). All these works are in agreement with Brønsted-Evans-Polanyi relationships, *i.e.* the higher the reaction energy, the lower the energy barriers [59].

Finally, results concerning the δ-MoC(001) surface are similar to those on β-C surface, where the exposure of surface C atoms seems to play a key role, rather than the particular surface Mo:C ratio. From Table 1 one readily sees that the energy barriers for H_2 dissociation are not affected by dispersion, being 0.60 and 0.64 eV, without and with dispersion, respectively. Note, however, that when neglecting dispersion, desorption becomes favored with respect to dissociation. This is not the case when accounting for dispersion, where dissociation is favored over desorption. Therefore, even for such a small and simple adsorbate, the effect of dispersion cannot be disregarded. We close this discussion by noting that the energy barrier for H_2 dissociation on the δ-MoC (001) surface is of the order of the value reported on TiC(001) [60,61] and ZrC(001) [62] surfaces, which have also a face centered cubic structure. This supports the effect of metal/C ratio on the catalyst activity, since the transition metal carbides with metal/C ratio of two present a higher activity than TMCs with a ratio of one [23,26].

In summary, vdW dispersion should be included when aiming at describing H_2 adsorption, dissociation, and H formation on the studied surfaces of Mo carbides, especially on δ-MoC (001) and β-C, where the H_2-surface interaction is especially weak.

3.2. Full coverage surface hydrogenation

From an experimental point of view, in order to carry out hydrogenation reactions, the amount of H_2 used is usually in excess [63,64]. Therefore, the catalyst surface is likely to be completely covered by H atoms and this situation needs to be considered as well. To this end, different coverages containing of 1, 2, 8, and 16 H adsorbed atoms on the (2×2) supercells have been tested. Note that this is slightly different from the situation studied by Wang et al. [28] where, on the same (2×2) supercells, up to 20 and 24 adsorbed H atoms were considered depending on the surface termination. In this work, we consider that a maximum coverage is reached by 16 adsorbed H atoms since the sequential H_2 dissociation steps necessarily need available surface active sites, and probably, higher energy barriers would be obtained for subsequent hydrogenation due to the fact that active sites would be already occupied by H atoms. The adsorption energy values *per* atom, listed on Table S4, indicate that the full coverage surface hydrogenation is favorable and shows that the adsorption energy *per* atom is practically the same whether the adsorption process includes 8 or 16 H atoms above the supercell. The most noticeable variations are detected on δ-MoC (001) surface.

Fig. 3 displays most stable β-Mo_2C structures after hydrogen adsorption at full coverage. In the case of the β-Mo surface, the H atoms occupy hollow Mo sites despite of the fact that on the co-adsorption of 2 and 8 H atoms, the most favorable site is the C_2 hollow [23], see Fig. 2a, in agreement with Wang et al. [28]. Probably this variation is due to the distribution of sites in the supercell surface model; β-Mo surface contains 8 hollow C_2 and 16 hollow Mo sites. If

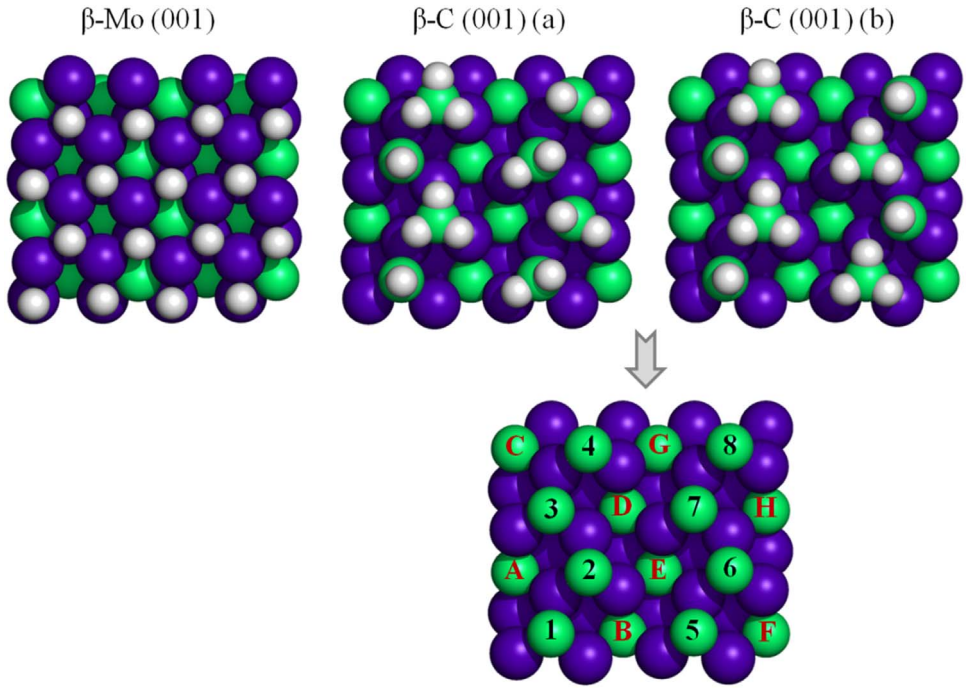

Fig. 3. Sketches on top view of full coverage hydrogenated β-Mo and β-C two degenerate structures. For β-C surface one can see the nomenclature of C atoms used on Table 3. Sphere coloring as in Fig. 2. (For interpretation of the references to color in this figure legend, the reader is referred to the web version of this article.)

the first 8 H atoms are adsorbed on hollow C_2, the rest of 8 H atoms should be adsorbed on hollow Mo and/or hollow C_1, increasing the H–H interaction owing to the H–H proximity. Nevertheless, the 16 H adsorption on Hollow Mo sites reduces this H–H interaction. On the other hand, C atoms at the second and fourth layer remain unchanged after β-Mo hydrogenation, and therefore, one can consider the C atoms in the same layer as equal by symmetry.

Regarding to the hydrogen adsorption on the β-C surface, the reconstruction detected at low coverages is also observed at 50% coverage (8H atoms). This is because after the H adsorption the surface energy of the reconstructed β-C is ~0.7 eV more stable than non-reconstructed surface, where the C displaced atoms are located on Hollow Mo^2 sites (see Fig. S1). Nevertheless, tests at full coverage —see Fig. S2— reveal that the most stable β-C surface is a non-reconstructed structure as one can see on Fig. 3. The full coverage hydrogenation on β-C surface leads to two degenerate structures even though both involve top C sites. The difference in these two different structures is on the distribution of CH, CH_2, and CH_3 groups; see Fig. 3. Note also that structure *A* contains the three kind of possible moieties whereas on *B*, only CH and CH_3 are present. Structure *A* is slightly more stable (~0.12 eV) than *B* although the adsorption energy *per* H atom is practically the same. In comparison to the study of Wang et al. [28], the

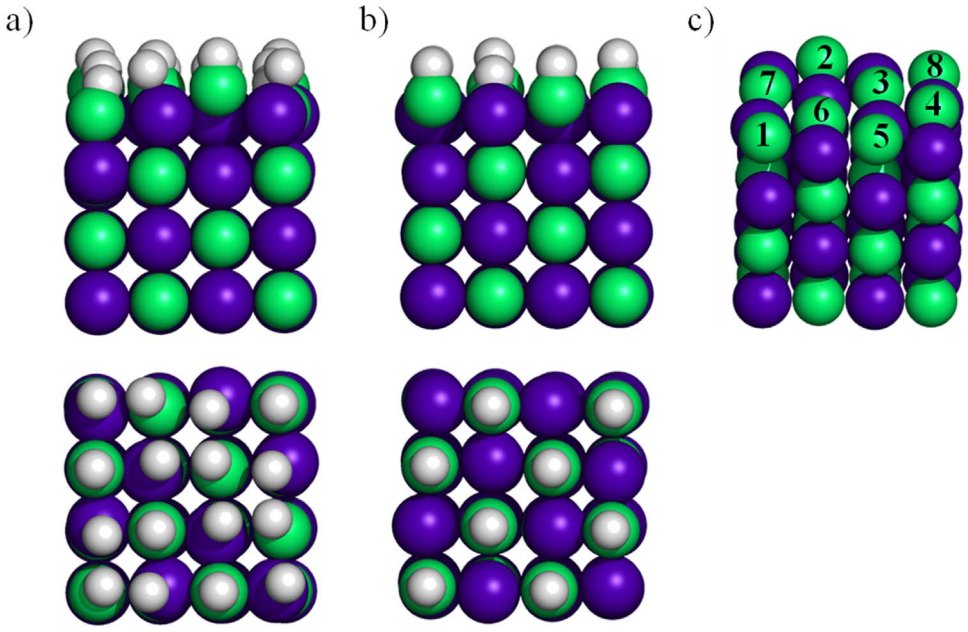

Fig. 4. Sketches on side view (top) and top view (bottom) of full coverage (a) and half coverage (b) hydrogenated δ-MoC (001) surface. Picture (c) shows the C surface nomenclature of 50% hydrogenated surface used on Table 4. Sphere coloring as in Fig. 2. (For interpretation of the references to color in this figure legend, the reader is referred to the web version of this article.)

stepwise adsorption of H atoms used by these authors lead to a situation where the 16 H atoms are located on top of C atoms, leading to the formation of CH_2 moieties. In the present work, this structure is ~0.3 eV less stable than the *A* structure and it has not been further considered. Geometries where only CH moieties are formed and the rest of H atoms are located on Hollow C and Mo sites, are ~2 eV higher in energy (see Fig. S2).

The particular distribution of H atoms implies that the environment around the surface C atoms is different and, consequently, the C(1*s*) CLBEs of these atoms could be different although whether the difference may be resolved remains an open question which we address in a forthcoming section. The difference in functionalized C atoms may also be visible by means of IR spectroscopy, considered later on. Besides, the different environment on C atoms located in the first atomic layer could also affect C atoms in the third layer. To facilitate the discussion, Fig. 3 presents the notation employed to distinguish the C atoms at the first and third atomic layers. Different atoms in the first layer are described by numbers and those of the third layer by capital letters. Fig. 4 displays full and half coverages of hydrogenated δ-MoC(001) surface, where H atoms occupy top-C and top-Mo sites. In the case of full H coverage, from the eight C–H bond thus formed, only four involve a significant (~1 Å) displacement of the C atoms along the vacuum direction. The reason behind this surface rumpling is simply to decrease the vicinal H–H repulsion. To proof that this is the case, calculations have been carried out hampering these C displacements. In this artificial structure, the total energy is 2 eV higher. On the other hand, in the half coverage situation, H adsorption occurs only on top of C surface atoms. Note that the C surface rumpling is not as pronounced as compared to full coverage situation. Due to stability reasons commented in the next subsection, the 50% H covered system is the key surface hydrogenated model of δ-MoC(001) surface. Following the notation used for the of β-C surface, the different surface C atoms of δ-MoC(001) are denoted using numbers. In the fully relaxed situation, the symmetry of C atoms in the first atomic layer is broken and one may wonder whether the distinct C atoms can be distinguished. For instance, the different C atoms may exhibit sufficiently large ΔCLBEs for the C 1*s* which shall be also discussed later on.

3.3. Relative stability of H-covered Mo_nC (001) surfaces

The largely exothermic adsorption energy values reported on Table S2 show that the presence of H atoms stabilize these surfaces. In the case of δ-MoC (001), the strong interaction implies a considerable surface rumpling. Nevertheless, from the adsorption energy values only it is not possible to establish the relative stability of surfaces with different H coverage situations. To estimate the relative stability of H-covered of β-C, β-Mo, and δ-MoC (001) surfaces, we rely on the calculated surface free energy of H covered (γ^{cover}) following the *ab initio* atomistic thermodynamics formalism described in the previous section and using values of hydrogen chemical potential $\left(\Delta\mu_{0_{H_2}}\right)$ at different working temperatures and pressures, and the pertinent surface free energy values.

Fig. 5 reports the calculated adsorption free energy of the three studied surfaces respect to the H coverage at different temperatures setting the external pressure to 5 atm, used in the past for catalytic hydrogentation reactions [24,26]. The results for all temperatures, pressures, and coverage conditions considered in the present work are listed in Table S5. From Fig. 5 one can first observe that increasing the temperature slightly destabilizes the surfaces. Note that for β-Mo_2C, independently of the surface termination, the surface stability increases with increasing H coverage at working conditions [23,24,26].

From the preceding discussion this fact is not so unexpected since H atoms adsorption on this surface result in the formation of strong C–H bonds in the case of β-C surface, and, in the case of β-Mo, the charge transfer from Mo to H atoms stabilizes the system—see Table S6. A slightly different situation is found for the δ-MoC (001) surface where it is stabilized up to half coverage, whereas further increasing of hydrogen coverage up to full coverage destabilizes the surface. This is simply because situation with H coverage higher than 50% involve H atoms at Mo sites; recall that H atoms are preferably bonded to C surface sites as observed on Table S3. Note that, on Table S6, the charge transfer from Mo to H is half with respect β-Mo.

Furthermore, the surface area is lower than on β-Mo_2C, which probably implies a superior H–H repulsion at higher coverages. On Table S5 one can check that at all tested pressures and temperatures, the γ^{cover}at half coverage present the lower values, and consequently, the simulation of characterization techniques carried out in the next sections has been performed using the 50% of covered surface model for δ-MoC and the full coverage model for β-Mo_2C surfaces. Finally, on Fig. S3, we display the Gibbs adsorption energy respect the pressure and temperature at the full coverage situation, where, for all tested surfaces, low temperatures and high pressures stabilize the full covered surfaces.

3.4. Analysis of the core level binding energy shifts

Table 2 reports the calculated ΔCLBEs values for the C 1*s* on β-Mo surface obtained at the initial state approximation on the bare and fully hydrogenated situations. Since the chemical environment affect ΔCLBEs, some structural data such as the C–H bond length have been added to the tables to provide geometric information about the origin of these shifts. Also, a comparison between calculations including or not the vdW terms reveal that the latter do not play any role on the calculated ΔCLBEs, differences being a constant shift for each surface of at most 0.09 eV.

For clean surfaces, all atoms in a given atomic layer are symmetrically equivalent and, hence, one single ΔCLBE value with respect to Mo_2C bulk is used for atoms in each atomic layer. For β-Mo surface, ΔCLBEs for the C atoms located at fourth layer are not shown since this in principle bulk-like layer is artificially in contact with vacuum. Here, ΔCLBEs for C atoms in the second layer are almost the same irrespective of the presence of adsorbed H atoms and, hence, within the limit of resolution even using synchrotron radiations which is ~0.1 eV [65].

A different situation is found for β-C (Table 3), where even for the clean surface noticeable shifts are predicted, which could be used to detect the presence of this termination. For the H-covered β-C surface, C–H bond formation leads to the noticeable ΔCLBEs with respect to bulk, but not so large when compared to the bare surface. Nevertheless, the formed CH, CH_2, and CH_3 like species have different ΔCLBEs which could be detected by XPS. Within the initial state approximation,

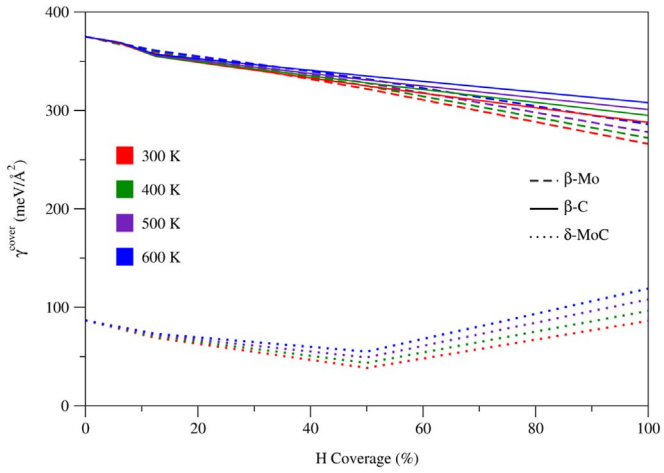

Fig. 5. Plots of surface free energy at H coverage (γ^{cover}) depending of the temperature at different H coverage at 5 atm of pressure.

Table 2
Core level binding energy shifts (ΔCLBEs) for C 1*s* on bare ($\Delta CLBE^b$) and fully hydrogenated ($\Delta CLBE^H$) situations for the β-Mo surface using the initial state approximation. The results are separated depending on whether vdW dispersion is included or not. All shifts are given in eV.

	non-vdW		vdW	
	$\Delta CLBE^b$	$\Delta CLBE^H$	$\Delta CLBE^b$	$\Delta CLBE^H$
2nd layer	−0.08	−0.21	−0.10	−0.24

the ΔCLBEs are negative. The larger shifts (~−1.1 eV) correspond to the C–H species whereas the smaller shifts (~−0.40 eV) corresponds to C bonded to three H atoms. The main difference between *A* and *B* geometries is the different ΔCLBEs for CH_2 species, which are not present on *B*. Eventually, one must take into account that both β-Mo and β-C terminations coexist and, unless using high resolution XPS, ΔCLBEs implying rather broad XPS peaks could be observably precluding the unequivocal assignment to a particular surface termination.

The ΔCLBEs values corresponding to the clean and half H-covered δ-MoC(001) surface are listed on Table 4. For the bare surface, ΔCLBEs calculated using the initial state approximation are close to the bulk for all relevant atomic layers. Upon hydrogenation, the ΔCLBEs with respect to δ-MoC bulk corresponding to C atoms located in the first atomic layer are negative and values for different types of C atoms, with different displacements on *z* axis direction, are probably not sufficiently different to allow experimental identification. No noticeable ΔCLBEs values are found for the C in deeper atomic layers.

3.5. Infrared spectra

In order to provide information that can be used in eventual experiments using IR spectroscopies, simulated IR spectra of each of the studied surfaces have been obtained. Fig. 6 reports all calculated spectra with those corresponding to the bare surface displayed on the left panels, and the fully hydrogenated surfaces on the right panels. In the view of all preceding results, simulated IR spectra have been obtained only without vdW dispersion. Let us to analyze the results in Fig. 6 in some detail. For the bare surfaces, one can distinguish peaks below to 1000 cm^{-1} region typically observed with Raman spectroscopies. More specifically, Mo related vibrations are located below 300 cm^{-1} whereas C related ones appear around 400–600 cm^{-1}. For the hydrogenated surfaces, one can observe small differences on the bare surface vibrations zone, probably, due to coupling to H related vibrational modes. The most remarkable peaks on δ-MoC (001) surface are the C–H symmetric (ν_s) and asymmetric stretching (ν_a) vibrations located at 2838 and 2824 cm^{-1}, respectively. Taking into account the obtained results on the previous sections, the half covered surface is the

Table 3
Core level binding energy shifts (ΔCLBEs) for C(1*s*) on bare ($\Delta CLBE^b$) and fully hydrogenated ($\Delta CLBE^H$) situations for the β-C surface using the initial state approximation. The results are separate depending on whether vdW dispersion is included or not. All shifts are given in eV. The C–H bond length, d(C–H), in Å, has been included to distinguish the different moieties and the bonding differences. The C nomenclature is as in Fig. 2. *A* and *B* correspond to the two different structures compatible with full coverage.

	non-vdW				vdW			
	$\Delta CLBE^b$	$\Delta CLBE^H$	Moiety	d(C–H)	$\Delta CLBE^b$	$\Delta CLBE^H$	Moiety	d(C–H)
Geometry A								
1st layer								
C^1	−0.71	−1.03	CH	1.11	−0.74	−1.05	CH	1.10
C^2		−0.43	CH_3	1.11/1.12/1.12		−0.41	CH_3	1.11/1.12/1.12
C^3		−1.03	CH	1.11		−1.05	CH	1.10
C^4		−0.43	CH_3	1.11/1.12/1.12		−0.41	CH_3	1.11/1.12/1.12
C^5		−0.51	CH_2	1.10/1.18		−0.55	CH_2	1.10/1.18
C^6		−0.74	CH_2	1.10/1.18		−0.77	CH_2	1.10/1.17
C^7		−0.51	CH_2	1.10/1.18		−0.55	CH_2	1.10/1.18
C^8		−0.73	CH_2	1.10/1.18		−0.77	CH_2	1.10/1.17
3rd layer								
C^A	−0.09	−0.13	–	–	−0.10	−0.13	–	–
C^B		−0.11	–	–		−0.11	–	–
C^C		−0.13	–	–		−0.13	–	–
C^D		−0.11	–	–		−0.11	–	–
C^E		−0.13	–	–		−0.14	–	–
C^F		−0.18	–	–		−0.18	–	–
C^G		−0.13	–	–		−0.14	–	–
C^H		−0.18	–	–		−0.18	–	–
Geometry B								
1st layer								
C^1	−0.71	−1.10	CH	1.10	−0.74	−1.12	CH	1.11
C^2		−0.40	CH_3	1.11/1.12/1.13		−0.38	CH_3	1.11/1.12/1.13
C^3		−1.10	CH	1.10		−1.12	CH	1.11
C^4		−0.40	CH_3	1.11/1.12/1.13		−0.38	CH_3	1.11/1.12/1.13
C^5		−0.45	CH_3	1.11/1.12/1.12		−0.44	CH_3	1.11/1.12/1.12
C^6		−0.93	CH	1.14		−0.95	CH	1.14
C^7		−0.44	CH_3	1.11/1.12/1.13		−0.44	CH_3	1.11/1.12/1.13
C^8		−0.92	CH	1.14		−0.94	CH	1.14
3rd layer								
C^A	−0.09	−0.22	–	–	−0.10	−0.22	–	–
C^B		−0.13	–	–		−0.14	–	–
C^C		−0.22	–	–		−0.23	–	–
C^D		−0.13	–	–		−0.13	–	–
C^E		−0.13	–	–		−0.14	–	–
C^F		−0.24	–	–		−0.25	–	–
C^G		−0.14	–	–		−0.14	–	–
C^H		−0.24	–	–		−0.25	–	–

Table 4
Core level binding energy shifts (ΔCLBEs) for C 1s on bare ($\Delta CLBE^{b}$) and hydrogenated ($\Delta CLBE^{H}$) for the δ-MoC(001) surface using the initial state approximation. The results are separate depending on whether vdW dispersion is included or not. All shifts are given in eV. For comparison, C–H and C–Mo bond lengths, d(C–H) and $d(C–Mo^{2})$, respectively, both in Å, are also reported. The C nomenclature is referred to Fig. 3.

	non-vdW				vdW			
	$\Delta CLBE^{b}$	$\Delta CLBE^{H}$	d(C–H)	$d(C–Mo^{2})$	$\Delta CLBE^{b}$	$\Delta CLBE^{H}$	d(C–H)	$d(C–Mo^{2})$
Initial state								
1st layer	−0.14				−0.14			
C^{1}		−0.42	1.11	2.30		−0.42	1.12	2.31
C^{2}		−0.66	1.12	2.65		−0.66	1.12	2.65
C^{3}		−0.42	1.11	2.31		−0.42	1.12	2.31
C^{4}		−0.67	1.12	2.65		−0.67	1.12	2.65
C^{5}		−0.72	1.12	2.85		−0.72	1.12	2.85
C^{6}		−0.67	1.12	2.68		−0.67	1.12	2.67
C^{7}		−0.73	1.12	2.85		−0.73	1.12	2.85
C^{8}		−0.67	1.12	2.67		−0.67	1.12	2.67
2nd layer	0.08	−0.17	–	–	0.08	−0.17	–	–
3rd layer	0.20	0.25	–	–	0.20	0.25	–	–

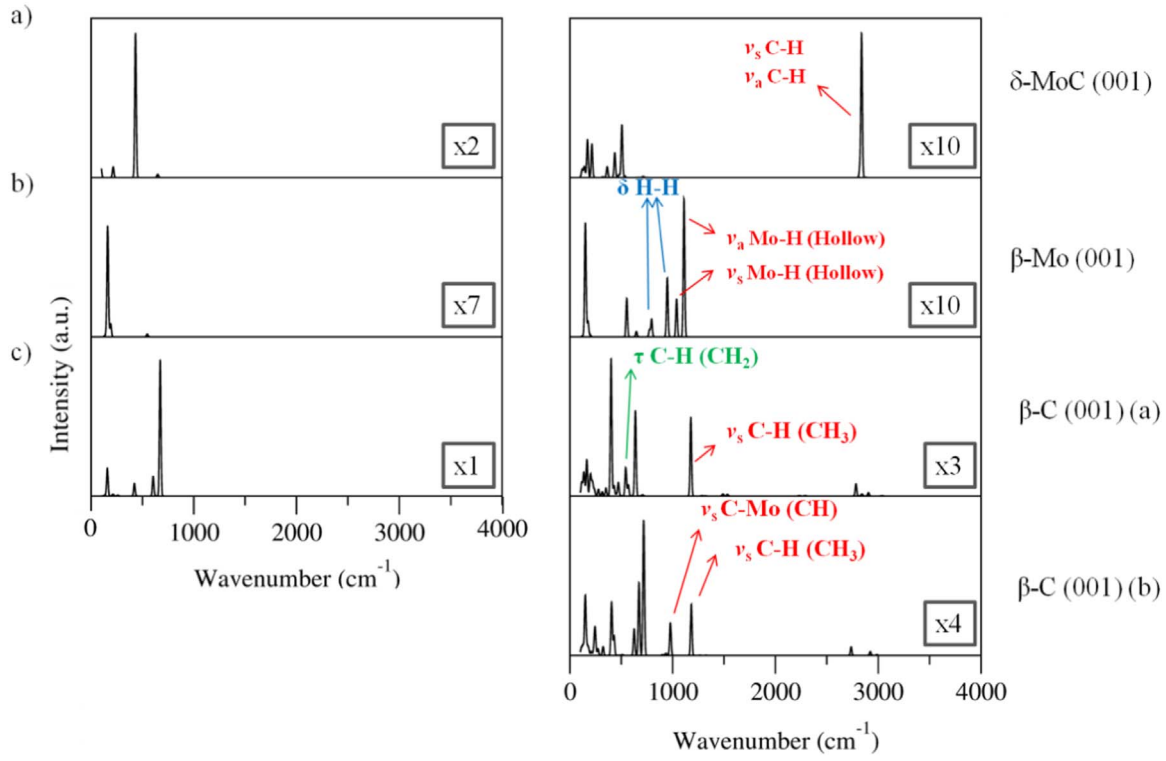

Fig. 6. Simulated IR spectra of bare (left) and fully hydrogenated, full coverage, (right) of δ-MoC (a), β-Mo (b), and β-C (c) (001) surfaces. The intensities have been enlarged by factor shown on the respective panels in order to improve the visualization.

most stable after H adsorption, without H atoms adsorbed on Mo surface atoms. However, the improbable adsorption of some H atoms on top Mo site could be detected by IR spectroscopy since, as one can see on Fig. S4 on the Supplementary material, the Mo–H asymmetric stretching (ν_a) appears at ~1730 cm^{-1} while the symmetric one (ν_s) at ~1755 cm^{-1}.

Logically, in the case of the β-Mo surface (Fig. 6b), the C–H stretching is not observed since H occupies hollow Mo atoms. This implies that Mo–H ν_s appears at ~1030 cm^{-1} and the ν_a at ~1100 cm^{-1}. These different bonding situations respect the possible (and improbable) adsorption of H atoms on δ-MoC (001) would be easily observed by IR experiments. At this surface, H bending (δ) is predicted to appear at around 750–900 cm^{-1}. On the β-C surface, the simulated IR spectra for both degenerate *A* and *B* structures have been performed. As one can see from Fig. 6, the spectra are very similar with a clear feature at 1176 cm^{-1} corresponding to the CH_3 ν_s. Furthermore, the C–H ν_s and ν_a of CH_3 surface species would appear at 2700–2900 cm^{-1} for both surface structures, yet with weak intensities. Finally, there are also slight differences such as the C–Mo stretching on C atoms bonded to one H, detected on geometry *B* at ~970 cm^{-1}, or the CH_2 moieties in geometry *A*, with a peak around 450–550 cm^{-1} corresponding to CH_2 twisting (τ), whereas on structure *B* there are no peaks at this region. Clearly, IR could provide information regarding the surface hydrogenation state.

4. Conclusions

Here an extensive theoretical study of the adsorption, dissociation, and formation of H_2 on cubic δ-MoC and orthorhombic β-Mo_2C (001) surfaces —the last one with C and Mo terminations —has been carried out at DFT level using the PBE functional including or not dispersion terms.

Results show that the energy profiles for the H_2 dissociation elementary steps are largely affected by dispersion. The calculations with vdW present an energy barrier essentially zero on β-Mo and β-C, and of 0.60 eV for δ-MoC, whereas calculations without vdW predict that on β-C and δ-MoC desorption would be more favorable than dissociation. The present calculations at low H coverage predict that for the three studied surfaces, H_2 dissociation is strongly exothermic, favoring dissociation against recombination. Taking into account the adsorption of one H_2 molecule on the (2×2) supercell, β-Mo_2C presents an essentially zero energy barrier for the H_2 dissociation, whilst the most appropriate for H_2 formation is δ-MoC. Surface free energy calculations reveal that both terminations of β-Mo_2C are stabilized with increasing H coverage. However, in the case of the δ-MoC (001) surface, H adsorption stabilizes up to half coverage where all C sites are occupied.

Regarding the simulation of properties which could be observed by means of usual surface characterization techniques, both XPS and IR are able to provide details of the surface structure before and after H deposition. The initial state core level binding energy shifts for C 1*s* indicate that it would be possible to distinguish many different environments around C atoms, such as CH, CH_2, and CH_3 moieties on β-C surface or the different C rumpling on δ-MoC triggered by C–H bond formation. Other minor changes have been detected through computational tools although these variations are below the resolution of XPS using synchrotron (0.1 eV). The different moieties produced after H adsorption —CH_3 (β-C) or CH (β-C and δ-MoC)— as well as the different H adsorption sites could be distinguished by means of IR experiments.

Acknowledgements

This manuscript has been authored by employees of Brookhaven Science Associates, LLC under Contract No. DE-SC0012704 with the U.S. Department of Energy. The research carried out at the *Universitat de Barcelona* was supported by the Spanish MINECO/FEDER grant CTQ2015-64618-R, and, in part, by *Generalitat de Catalunya* (grants 2014SGR97 and XRQTC) and from the NOMAD Center of Excellence Project; the latter project has received funding from the European Union Horizon 2020 Research and Innovation Programme under grant agreement No. 676580. S.P.P. acknowledges financial support from Spanish MEC predoctoral grant associated to CTQ2012-30751. F.V. thanks the MINECO for his postdoctoral *Ramón y Cajal* (RyC) research contract (RYC-2012-10129) and F.I. acknowledges additional support from the 2015 ICREA Academia Award for Excellence in University Research. Computational time at the *MARENOSTRUM* supercomputer has been provided by the Barcelona Supercomputing Centre (BSC) through a grant from *Red Española de Supercomputación* (RES).

Appendix A. Supplementary material

Supplementary data associated with this article can be found in the online version at http://dx.doi.org/10.1016/j.susc.2016.10.001.

References

[1] R.B. Levy, M. Boudart, Science 181 (1973) 547.
[2] H.H. Hwu, G. Chen, Chem. Rev. 105 (2005) 185.
[3] A.L. Stottlemyer, T.G. Kelly, Q. Meng, J.G. Chen, Surf. Sci. Rep. 67 (2012) 201.
[4] M.D. Porosoff, X. Yang, J.G. Chen, Energy Environ. Sci. 9 (2016) 62.
[5] M.M. Sullivan, C.J. Chen, A. Bhan, Catal. Sci. Technol. 6 (2016) 602.
[6] J.G. Chen, Surf. Sci. Rep. 30 (1997) 1.
[7] J.G. Chen, Chem. Rev. 96 (1996) 1477.
[8] S.T. Hunt, M. Milina, A.C. Alba-Rubio, C.H. Hendon, J.A. Dumesic, Y. Román-Leshkov, Science 352 (2016) 974.
[9] Y.N. Regmi, G.R. Waetzig, K.D. Duffee, S.M. Schmuecker, J.M. Thode, B.M. Leonard, J. Mater. Chem. A 3 (2015) 10085.
[10] J.J. Liao, R.C. Wilcox, R.H. Zee, Scr. Metall. Mater 24 (1990) 1647.
[11] J.A. Nelson, M.J. Wagner, Chem. Mater. 14 (2002) 4460.
[12] M.D. Porosoff, M.N.Z. Myint, S. Kattel, Z. Xie, E. Gomez, P. Liu, J.G. Chen, Angew. Chem. Int. Ed. 54 (2015) 15501.
[13] J.A. Rodriguez, P. Liu, Y. Takahashi, K. Nakamura, F. Viñes, F. Illas, J. Am. Chem. Soc. 131 (2009) 8595.
[14] J.A. Rodriguez, P.J. Ramírez, G.G. Asara, F. Viñes, J. Evans, P. Liu, J.M. Ricart, F. Illas, Angew. Chem. Int. Ed. 53 (2014) 11270.
[15] T.P. Saint Clair, S.T. Oyama, D.F. Cox, S. Otani, Y. Ishizawa, R.L. Low, K. Fukui, Y. Iwasawa, Surf. Sci. 426 (1999) 187.
[16] C. Jimenez-Orozco, E. Florez, A. Moreno, P. Liu, J.A. Rodriguez, J. Phys. Chem. C 120 (2016) 13531.
[17] P. Liu, J.A. Rodriguez, J. Phys. Chem. B 110 (2006) 19418.
[18] N.M. Schweitzer, J.A. Schaidle, O.K. Ezekoye, X. Pan, S. Linic, L.T. Thompson, J. Am. Chem. Soc. 133 (2011) 2378.
[19] Y. Liu, J. Ding, J. Sun, J. Zhang, J. Bi, K. Liu, F. Kong, H. Xiao, Y. Sun, J. Chen, Chem. Commun. 52 (2016) 5030.
[20] Y. Shi, Y. Yang, Y.W. Li, H. Jiao, Catal. Sci. Technol. 6 (2016) 4923.
[21] R. Barthos, F. Solymosi, J. Catal. 249 (2007) 289.
[22] M.D. Porosoff, X. Yang, J.A. Boscoboinik, J.G. Chen, Angew. Chem. Int. Ed. 53 (2014) 6705.
[23] S. Posada-Pérez, F. Viñes, P.J. Ramirez, A.B. Vidal, J.A. Rodriguez, F. Illas, Phys. Chem. Chem. Phys. 16 (2014) 14912.
[24] S. Posada-Pérez, P.J. Ramirez, R.A. Gutierrez, D.J. Stacchiola, F. Viñes, P. Liu, F. Illas, J.A. Rodriguez, Catal. Sci. Technol. doi: ⟨http://doi.org/10.1039/c5cy02143j⟩.
[25] L. Li, D.S. Sholl, ACS. Catal. 5 (2015) 5174.
[26] S. Posada-Pérez, P.J. Ramírez, J. Evans, F. Viñes, P. Liu, F. Illas, J.A. Rodríguez, J. Am. Chem. Soc. 138 (2016) 8269.
[27] A. Vojvodic, Catal. Lett. 142 (2012) 728.
[28] T. Wang, X. Tian, Y. Yang, Y.W. Li, J. Wang, M. Beller, H. Jiao, Surf. Sci. 651 (2016) 195.
[29] K. Reuter, M. Scheffler, Phys. Rev. B 65 (2002) 035406.
[30] K. Reuter, M. Scheffler, Phys. Rev. Lett. 90 (2003) 046103.
[31] Powder Diffraction File, JCPDS International Center for Diffraction Data, Pennsylvania, 2004.
[32] J.Rd.S. Politi, F. Viñes, J.A. Rodriguez, F. Illas, Phys. Chem. Chem. Phys. 15 (2013) 12617.
[33] J.W. Han, L.W. Li, D.S. Sholl, J. Phys. Chem. C 115 (2011) 6870.
[34] J. Ren, C.-F. Huo, J. Wang, Z. Cao, Y.-W. Li, H. Jiao, Surf. Sci. 600 (2006) 2329.
[35] H. Tominaga, Y. Aoki, M. Nagai, Appl. Catal. A 423–424 (2012) 192.
[36] H. Tominaga, M. Nagai, J. Phys. Chem. B 109 (2005) 20415.
[37] A.N. Christensen, Acta Chem. Scand. Ser. A 31 (1977) 509.
[38] E. Parthé, V. Sadagopan, Acta Crystallogr. 16 (1963) 202.
[39] J.P. Perdew, K. Burke, M. Ernzerhof, Phys. Rev. Lett. 77 (1996) 3865.
[40] S. Grimme, J. Comput. Chem. 27 (2006) 1787.
[41] P.E. Blöch, Phys. Rev. B 50 (1994) 17953.
[42] G. Kresse, D. Joubert, Phys. Rev. B 59 (1999) 1758.
[43] H.J. Monkhorst, J.D. Pack, Phys. Rev. B: Solid State 13 (1976) 5188.
[44] G. Henkelman, H. Jonsson, J. Chem. Phys. 111 (1999) 7010.
[45] F. Viñes, A. Iglesias-Juez, F. Illas, M. Fernández-García, J. Phys. Chem. C 118 (2014) 1492.
[46] G. Kresse, J. Hafner, Phys. Rev. B 47 (1993) 558.
[47] S. Posada-Pérez, J.R.d.S. Politi, F. Viñes, F. Illas, RSC Adv. 5 (2015) 33737.
[48] T. Wang, X. Liu, S. Wang, C. Huo, Y.W. Li, J. Wang, H. Jiao, J. Phys. Chem. C 115 (2011) 22360.
[49] N.H. Moreira, G. Dolgonos, B. Aradi, A.L. da Rosa, T. Frauenheim, J. Chem. Theory. Comput. 5 (2009) 605.
[50] C.G. Tang, M.J.S. Spencer, A.S. Barnard, Phys. Chem. Chem. Phys. 16 (2014) 22139.
[51] P.S. Bagus, Phys. Rev. 139 (1965) A619.
[52] P.S. Bagus, E.S. Ilton, C.J. Nelin, Surf. Sci. Rep. 68 (2013) 273.
[53] P.S. Bagus, F. Illas, G. Pacchioni, F.J. Parmigiani, Electron. Spectrosc. Relat. Phenom. 100 (1999) 215.
[54] D.P. Chong, E.J. Gritsenko, E.J. Baerends, J. Chem. Phys. 116 (2002) 1760.
[55] M. Segala, Y. Takahata, D.P. Chong, J. Electron. Spectrosc. Relat. Phenom. 151 (2006) 9.
[56] N. Pueyo-Bellafont, P.S. Bagus, F. Illas, J. Chem. Phys. 142 (2015) 214102.
[57] L. Köhler, G. Kresse, Phys. Rev. B 70 (2004) 165405.
[58] T. Wang, Y.W. Li, J. Wang, M. Beller, H. Jiao, J. Phys. Chem. C 118 (2014) 8079.
[59] F. Viñes, A. Vojvodic, F. Abild-Pedersen, F. Illas, J. Phys. Chem. C 117 (2013) 4168.
[60] S. Posada-Pérez, F. Viñes, J.A. Rodriguez, F. Illas, Top. Catal. 58 (2015) 159.
[61] F. Viñes, J.A. Rodriguez, P. Liu, F. Illas, J. Catal. 260 (2008) 103.
[62] E. Florez, T. Gomez, J.A. Rodriguez, F. Illas, Phys. Chem. Chem. Phys. 13 (2011) 6865.
[63] S.D. Senanayake, P.J. Ramírez, I. Waluyo, S. Kundu, K. Musiyanselage, Z. Liu, Z. Liu, S. Axnanda, D.J. Stacchiola, J. Evans, J.A. Rodriguez, J. Phys. Chem. C 120 (2016) 1778.
[64] J.A. Rodriguez, J. Evans, L. Feria, A.B. Vidal, P. Liu, K. Nakamura, F. Illas, J. Catal. 307 (2013) 162.
[65] A. Baraldi, J. Phys.: Condens. Matter 320 (2008) 86.